



## A Root-Locus Design Methodology Derived from the Impedance/Admittance Stability Formulation and Its Application for LCL Grid-Connected Converters in Wind Turbines

Freijedo Fernandez, Francisco Daniel; Diaz, Enrique Rodriguez; Golsorkhi, Mohammad; Quintero, Juan Carlos Vasquez; Guerrero, Josep M.

*Published in:*  
I E E E Transactions on Power Electronics

*DOI (link to publication from Publisher):*  
[10.1109/TPEL.2016.2645862](https://doi.org/10.1109/TPEL.2016.2645862)

*Publication date:*  
2017

*Document Version*  
Early version, also known as pre-print

[Link to publication from Aalborg University](#)

*Citation for published version (APA):*  
Freijedo Fernandez, F. D., Diaz, E. R., Golsorkhi, M., Quintero, J. C. V., & Guerrero, J. M. (2017). A Root-Locus Design Methodology Derived from the Impedance/Admittance Stability Formulation and Its Application for LCL Grid-Connected Converters in Wind Turbines. *I E E E Transactions on Power Electronics*, 32(10), 8218 - 8228 .  
<https://doi.org/10.1109/TPEL.2016.2645862>

### General rights

Copyright and moral rights for the publications made accessible in the public portal are retained by the authors and/or other copyright owners and it is a condition of accessing publications that users recognise and abide by the legal requirements associated with these rights.

- Users may download and print one copy of any publication from the public portal for the purpose of private study or research.
- You may not further distribute the material or use it for any profit-making activity or commercial gain
- You may freely distribute the URL identifying the publication in the public portal -

### Take down policy

If you believe that this document breaches copyright please contact us at [vbn@aub.aau.dk](mailto:vbn@aub.aau.dk) providing details, and we will remove access to the work immediately and investigate your claim.

# A Root-Locus Design Methodology Derived from the Impedance/Admittance Stability Formulation and Its Application for LCL Grid-Connected Converters in Wind Turbines

Francisco D. Freijedo, *Senior Member, IEEE*, Enrique Rodriguez-Diaz, *Student Member, IEEE*, Mohammad S. Golsorkhi, *Student Member, IEEE*, Juan C. Vasquez, *Senior Member, IEEE* and Josep M. Guerrero, *Fellow Member, IEEE*

**Abstract**—This paper presents a systematic methodology for design and tuning of the current controller in LCL grid-connected converters for wind turbine applications. The design target is formulated as a minimization of the current loop dominant time constant, which is in accordance with standard design guidelines for wind turbine controllers (fast time response and high stability margins). The proposed approach is derived from the impedance/admittance stability formulation, which, on one hand, has been proved to be suitable for controller design when active damping is implemented and, on the other hand, it has been also proved to be very suitable for system level studies in applications with a high penetration of renewable energy resources. The tuning methodology is as follows: firstly, the physical system is modelled in terms of the converter admittance and its equivalent grid impedance; then, a sensitivity transfer function is derived, from which the closed-loop eigenvalues can be calculated; finally, the set of control gains that minimize the dominant time constant are obtained by direct search optimization. A case study that models the target system in a low power scale is provided and experimental verification validates the theoretical analysis. More specifically, it has been found that the solution that solves the minimization of the current controller time constant (wind turbine controller target) also corresponds to a highly damped electrical response (robustness provided by the active damping).

**Index Terms** - Ac/dc power conversion, active damping, current control, pulse width modulation converters, stability, wind power generation.

## I. INTRODUCTION

Failures of the electric conversion system have an important influence in the number of downtime hours per year [1]. Therefore, robust design of the wind turbine controllers to properly work in different scenarios has a beneficial effect in terms of reliability and availability. Industrial wind turbine controllers are complex multi-loop structures, which involve both mechanical and electric actuators [2]–[5]. The top level design guidelines that apply for wind turbine controllers set the dynamic requirements for each loop in terms of a maximum

value for its dominant time constant [4], [5]. This is in agreement with basic theory for cascaded loop design: a short time constant of an inner controllers is convenient for the dynamics of its outer loops [6], [7]. Since the current controllers are the innermost loops of the whole wind turbine controller [8], the time constant minimization of this loops is the control objective that better fits with the wind turbine application [9]–[11]. Furthermore, fast dynamics is also demanded to accomplish stringent grid-code requirements in faulty/weak grid situation [9], [10], [12], [13].

On the other hand, LCL output filter configuration is employed in order to improve the filtering of switching harmonics and fulfil harmonic standards in type IV wind turbines [14]. The selection of filter parameters is not a trivial task, as the internal resonance affects to the current controller dynamics [15]–[24]. Active and passive damping techniques have been proposed for a better dynamic behavior: the goal is to mitigate the harmonic amplification effects around the resonance frequency. In principle, passive damping is unwanted as it is associated to an efficiency loss [15]. Active damping techniques, on the contrary, mitigate the effects of the LCL resonance by proper control actions [16]–[24]. The use of a filtered voltage feed-forward (i.e., use the capacitor voltage in an innermost loop) for active damping [16], [17], [20], [24] can be considered a convenient solution for wind turbine applications, because of its simplicity and readiness (e.g., little modifications to the control structure, no extra sensors needed), and therefore, this technique is considered in this work.

The main objective of this paper is to provide a systematic design approach, which addresses the main control objectives of minimizing the dominant time constant from a constrained system definition (the hardware design is mainly imposed by the wind turbine transformer [14], [25]). The impedance/admittance stability criterion [26], [27] is used to formulate the control problem: the converter dynamics are expressed by an equivalent converter admittance; the LCL capacitance branch in combination with the transformer leakage set the grid impedance [17], [20], [27]. Subsequently, from this formulation an equivalent nominal sensitivity transfer function is proposed. It is shown as the root-locus of this equivalent nominal sensitivity provides the location of the closed-loop poles. Then, from a parametric analysis, it is possible to select the

Manuscript received January 25, 2016; revised March 29, 2016, June 28, 2016 and October 18, 2016; accepted December 22, 2016.

This work was partially supported by energiforskning.dk and the Aalborg University through the iDClab project (3045-00010B).

Francisco D. Freijedo is with the Power Electronics Lab, Ecole Polytechnique Federale de Lausanne, CH1005, Lausanne, Switzerland. E-mail: francisco.freijedo@epfl.ch.

Enrique Rodriguez-Diaz, Juan C. Vasquez and Josep M. Guerrero are with the Department of Energy Technology, Aalborg University, 9220 Aalborg East, Denmark. E-mails: {erd,juq,joz}@et.aau.dk.

Mohammad S. Golsorkhi is with the Department of Electrical and Electronic Engineering, the University of Hong Kong, Hong Kong. E-mail: sadagh5@eee.hku.hk.

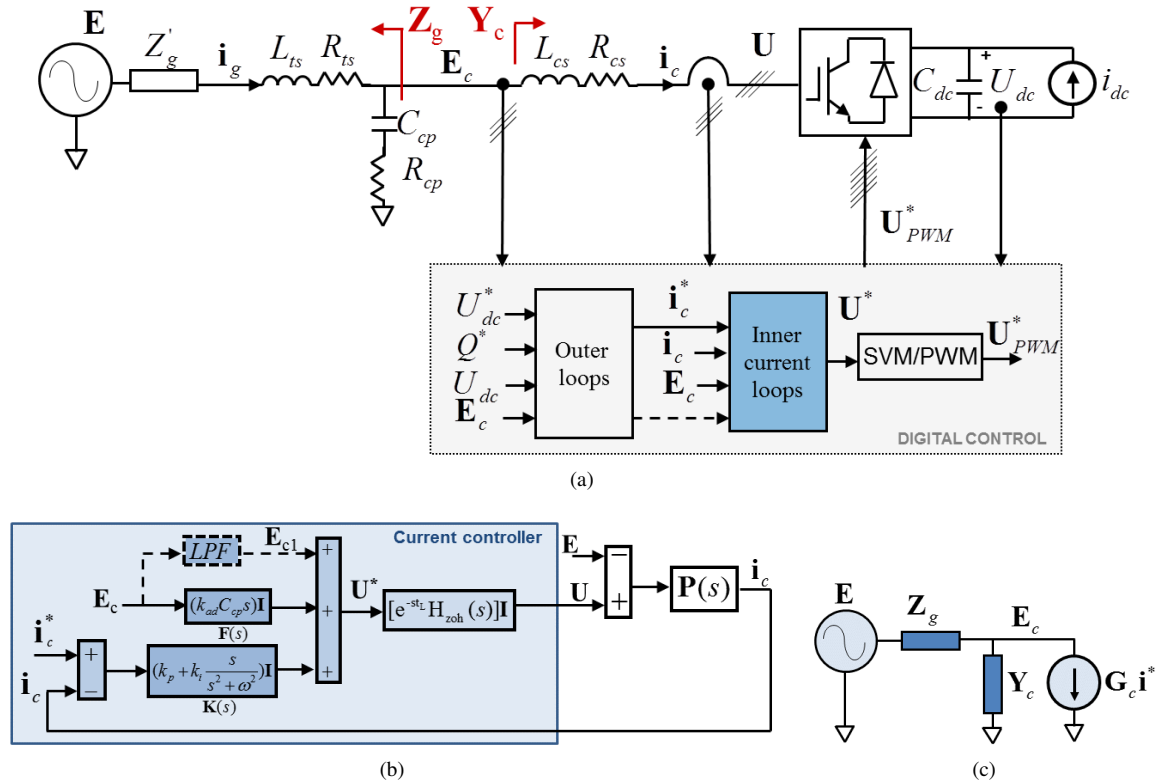


Fig. 1. System description. (a) LCL grid-connected VSC converter. (b) Current controller. (c) Admittance/Impedance formulation for dynamics assessment.

main control and active damping parameters to accomplish the control objectives: 1) maximizing the dominant time constant and 2) minimize harmonic interactions around the resonance frequency. Both objectives can be described analytically by the position of the dominant poles [11]. Therefore, an optimal solution to the tuning problem can be found by a direct search of the controller parameters that maximize the absolute value of the real part of the system dominant poles.

The developed impedance/admittance root locus provides advantages in comparison with the formulations derived from the classical closed loop schemes, such as the analyses of [9], [16], [19]: from the control design point of view, the active damping action is modeled as a part of the converter admittance, which avoids the analysis of multiple-loop structures [17], [20], [28]. Furthermore, the ability of modeling the converter by its equivalent admittance permits to include its behavior in wind farm system level studies [29], [30]; therefore, a customized tuning of the wind turbine as a function of its placement inside the wind power plant is feasible, which poses an interesting analysis for further works.

In comparison to previous works based on the impedance/stability formulation [20], [27], [28], this work provides a quantitative solution for the wind turbine controller design flow (i.e., the value of the current loop time constant). The proposed method also provides a solution with high relative stability: from the definition of the problem, the dominant poles are placed in a constrained stability region of the root-locus, which is a good measure of robustness in the presence of physical system uncertainties [31], [32]. In this sense, it is more restrictive than designs for passivity methods

[20], [28], [33], since solutions associated to closed-loop poles near the right half plane (RHP) are not allowed (by definition of a constrained stability region). On the other hand, the downside of the proposed method in comparison to design for passivity is that a nominal grid model is needed for the tuning. However, in practice, the nominal grid model (as seen by the converter) is well defined by the LCL filter, for which the parameters are known. This discussion suggests that a comparative between both techniques in terms of sensitive analyses in a realistic scenario (e.g., using real data from an existing wind power plant) is a potential work to be addressed in future.

The rest of the paper is organized as follows. Section II describes the LCL grid-connected converter circuit, the current controller and the basics of the impedance/admittance formulation. Section III describes the controller implementation details and how they are modeled. Section IV shows the methodology for the root-locus derivation and how it is aligned with the overall design objectives. Section V develops a case study using the lab-scale prototype parameters that are subsequently employed in Section VI for experimental validation. Finally, the paper is concluded by summarizing the main outcomes and contributions.

## II. SYSTEM DESCRIPTION AND MODELING

### A. Circuit Modeling

Fig. 1(a) represents a LCL grid-connected VSC working in current control mode. The voltages  $E$  and  $U$  represent the stiff grid and VSC output voltage, respectively. The LCL

output filter is formed by the converter side inductive filter, the capacitance and transformer leakage model. The converter side filter is defined by series inductance  $L_{cs}$  and resistance  $R_{cs}$ . The capacitance is given by a parallel capacitance  $C_{cp}$  in series with a small equivalent series resistor  $R_{cp}$ . The transformer model is given by a leakage inductance  $L_{ts}$  and a leakage resistor  $R_{ts}$  in series. The voltage across the capacitor branch is  $E_c$ . This point defines the converter point of connection for the proposed Impedance/Admittance stability analysis. The grid impedance is represented by  $Z'_g$ , which depends on power system circuit and grid conditions [21], [34].

Focusing on a type IV wind turbine application, the biggest constraint in the hardware design is imposed by the transformer short-circuit current [25], which in practice sets  $L_{ts}$  [14]. Typical values for the secondary inductance are then in the range  $[0.06, 0.1]$  p.u. of the machine rate power [14], [35]. Following LCL design basic guidelines, the secondary inductance also constraints the selection of the converter filter: a primary inductance equal to the transformer inductance is a reasonable design both in terms of cost and dc-bus usage [14], [16]. Using  $L_{ts}$  as a constraint (which may include the inductive part of  $Z'_g(s)$  if available [14]), in practice, the main degree of freedom of the LCL filter is the choice of the capacitance  $C_{cp}$ . The LCL resonance frequency (angular) is given by

$$\omega_{res} = \sqrt{\frac{L_{cs} + L_{ts}}{L_{cs}L_{ts}C_{cp}}}. \quad (1)$$

The selection of  $\omega_{res}$  involves a trade-off between control interactions and enhanced filtering [15], [16], [19], [36]. From the point of view of the capacitor based active damping, typical values at which the technique is more effective are in the range of  $[0.1\omega_s, 0.2\omega_s]$ , with  $\omega_s$  being the angular sampling frequency [16].

The role of the resistive components is also worth mentioning. From the VSC efficiency perspective, these are associated to system power losses. However, from the control point of view, they are beneficial as they damp the dynamics of the closed loop system [15], [16].

### B. Current Controller Structure

Fig. 1(b) shows the analyzed controller structure.  $K(s)$  represents the main controller, which in this work is a PR implemented in  $\alpha\beta$ -frame

$$\mathbf{K}(s) = (k_p + k_i \frac{s}{s^2 + \omega^2})\mathbf{I} \quad (2)$$

with  $k_p$  and  $k_i$  being the proportional and resonant gains, respectively.  $\mathbf{I}$  represents a  $2 \times 2$  unity matrix, which means that  $\mathbf{K}(s)$  is diagonal, which eases the dynamics assessment [11]. The PR controller is suitable for cascaded loop controllers in wind turbine applications: one key advantage is that it is a simple structure with ability to control the negative-sequence [8], [9], which is becoming an interesting feature for grid-codes compliance [2].

The control action calculation also includes an  $E_c$  voltage feedforward double path [see Fig. 1(b)], with the following

objectives: 1) provide a filtered value of the main grid component to improve the initial transient [28] and 2) an active damping action based on capacitor voltage derivative term [16], [20], [24]. The active damping action is given by the  $E_c$  path through a feedforward filter defined as

$$\mathbf{F}(s) = (k_{ad}C_{cp}s)\mathbf{I}. \quad (3)$$

with  $k_{ad}$  being the active damping gain ( $C_{cp}$  is the capacitor nominal value).  $\mathbf{F}(s)$  is also diagonal.

The system delay is modeled by a time latency  $t_L$  due to discrete-time operation (e.g., A/D and D/A conversion times of the digital board) and half a control sample due to PWM [zero order hold (ZOH)] operation [10], [11], [20]. Even both blocks are usually merged in one pure delay one, it has been found that splitting the delay model in two transfer functions better matches the whole frequency response around  $\omega_{res}$ .

The system plant is represented by  $P(s)$ , which is a function of the LCL filter components [and  $Z'_g(s)$ ] [16], [18], [19].

Until now, the matrix notation in the figure represents the three-phase and scalar variables of the real circuit. Subsequently, for the sake of generality scalar notation is used, as no couplings between phases are considered. This assumption is accurate since the proposed controller (implemented in  $\alpha\beta$ -frame) and the plant are diagonal [37], [38].

### C. Admittance/Impedance formulation for dynamics assessment of grid-connected VSCs

Fig. 1(c) shows an alternative formulation of the grid-connected current controlled VSC problem. The digital controller and the converter-side filter (formed by  $L_{cs}$  and  $R_{cs}$ ), which are well parametrized during the design stage, are modeled by an equivalent admittance  $Y_c(s)$  [and the closed loop gain  $G_c(s)$  which sets the dependence on the current reference]. The converter dynamics are set by the admittance interacting with the rest of grid impedances, grouped in  $Z_g(s)$ ; i.e., the  $Y_c(s)Z_g(s)$  Nyquist trajectories set the dynamics of the system [20], [27], [39], [40].

A key feature of the Impedance/Admittance formulation is that  $Y_c(s)$  definition includes all the  $E_c(s)$  internal feedback paths, which eases the study of active damping [17], [20], [28]. The explicit derivations of  $Y_c(s)$  and  $Z_g(s)$  are given in the following.

From Fig. 1(a), the converter admittance transfer function is defined by the ratio  $i_c(s)$  over  $E_c(s)$ , with  $E_c(s)$  being defined as an ideal voltage source and the current reference set to zero [the closed loop gain  $G_c(s)$  can be defined in a similar manner], i.e.,

$$Y_c(s) = \left. \frac{i_c(s)}{E_c(s)} \right]_{i_c^*=0} \left( \left. G_c(s) = \frac{i_c(s)}{i_c^*(s)} \right]_{E_c=0} \right). \quad (4)$$

$Y_c(s)$  can be also identified as the converter current due to the grid voltage acting as a disturbance (i.e., effect of grid voltage harmonics in the current loop) [9], [20].

By considering both circuit and current control equations, analytical expressions for  $Y_c(s)$  can be obtained [20], [28];

i.e., from Fig. 1(a) and Fig. 1(b),

$$Y_c(s) = \frac{1 - F(s) e^{-st_L} H_{zoh}(s)}{L_{cs}s + R_{cs} + K(s) e^{-st_L} H_{zoh}(s)}. \quad (5)$$

It should be remarked that  $Y_c(s)$  is a function of the interface filter in combination with the controller (including system delays) transfer functions. The effect of outer loops, such as phase-locked loop, dc-link or reactive power control, in  $Y_c(s)$  can be neglected as in practice the bandwidth of those outer loops should be much smaller than  $\omega_{res}$  [39]–[42]. Using a similar reasoning, the feedforward path filtering  $E_{c1}$  from  $E_c$  to improve the grid-connection initial transient [see Fig. 1(b)] can be also neglected [28].

On the other hand, the grid impedance as seen from the  $E_c(s)$  point is given by the capacitance filter connected in parallel to the transformer leakage impedance; i.e.,

$$Z_g(s) = Z_{gp}(s) // Z_{gs}(s) \quad (6)$$

with

$$Z_{gp}(s) = 1/(C_{cp}s) + R_{cp} \quad (7)$$

and

$$Z_{gs}(s) = L_{ts}s + R_{ts} + Z'_g(s). \quad (8)$$

### III. IMPLEMENTATION DETAILS AND ITS MODELING IN THE S-DOMAIN

This section refers to the main discrete-time implementation details and how these blocks are modeled in the continuous domain. Overall, it is sought to use low order expressions that well fit the actual frequency response up to  $\omega_{res}$ .

#### A. System Modeling of Delays

The system latency represents pure delays in the systems, such as A/D conversion. This delay can be approximated by the first order expression

$$e^{-t_L s} = \frac{e^{-t_L s/2}}{e^{t_L s/2}} \approx \frac{1 - st_L/2}{1 + st_L/2} \quad (9)$$

which provides unitary amplitude and good phase matching up to  $0.2\omega_s$  [11].

Even the ZOH is usually modeled by half a sample delay, it introduces some amplitude correction. The exact expression of ZOH transfer function is given by

$$H_{zoh}(s) = \frac{1 - e^{-s/f_s}}{s/f_s}. \quad (10)$$

with  $f_s$  being the sampling frequency. Using the same approximation for the delay that in (9), the ZOH can be approximated by a first order expression

$$H_{zoh}(s) \approx \frac{1}{1 + s/(2f_s)} \quad (11)$$

which well matches amplitude and phase in a low frequency range up to  $0.2\omega_s$ .

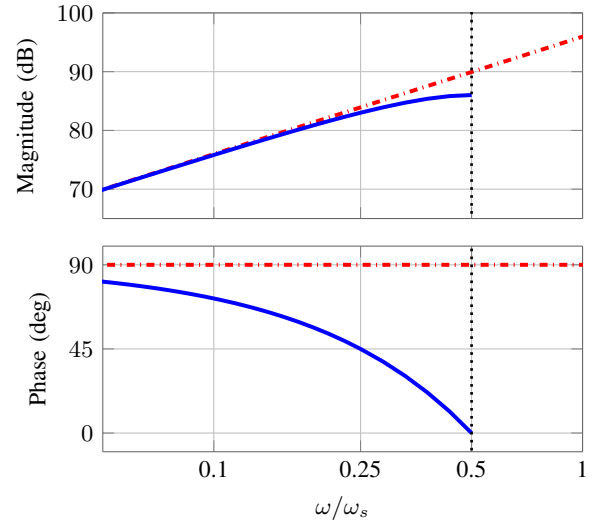


Fig. 2. Frequency response of time derivative filters: (solid blue) discrete filter obtained from the backward-difference rule; (dashed-dotted red) ideal filter (anti-causal);  $\omega_s = 2\pi f_s$  with  $f_s = 10$  kHz is represented.

#### B. Controller Filters

For the discrete-time implementation, the impulse invariant method has been used for the resonant filter of  $K(s)$ . The discrete PR controller is

$$K(z) = k_p + k_i \frac{z^2 - 1 \cos(\omega/f_s) z^1}{z^2 - 2 \cos(\omega/f_s) z^1 + 1} \quad (12)$$

This implementation well matches the continuous-domain definition [9], [10], [43], and hence the continuous domain expression well represents the real implementation; i.e., (2) is employed to calculate the root-loci.

However, the situation is not so straightforward for the active damping path. The implementation of an ideal differentiation filter is not available, as it is a non proper transfer function (i.e., a noncausal filter) [32]. Different approximation giving to discrete-domain causal filters are available [16], [24], [32]. A simple, first order approximation for the discrete-time derivative is obtained by the backward-difference rule [32] as follows

$$s \rightarrow \frac{f_s(z-1)}{z}. \quad (13)$$

From (13), the discret derivative action is performed by a causal filter, which has a zero at the origin and a pole at  $\omega_s/2$ . Fig. 2 shows the frequency response of the discrete-derivative filter and compares with the ideal anti-causal implementation: as frequency increases, the phase-angle and amplitude are reduced, which means that the discrete differentiator losses its properties at frequencies near the Nyquist frequency. This filter behaves as derivative up to  $0.25\omega_s$  (i.e., its phase is between 45 deg and 90 deg), with  $\omega_{res} < 0.25\omega_s$  being a reasonable practical assumption (at higher frequencies, the acquisition anti-aliasing filters tend to make the control action ineffective [44]). Therefore, it is expected that the discrete derivative defined by (13) is a reasonable solution for active damping based on voltage feedforward. According to the latest implementation assumption, the active damping filter in the

discrete domain is given by

$$F(z) = k_{ad}C_{cp} \frac{f_s(z-1)}{z}. \quad (14)$$

By noting that  $z = e^{s/f_s}$  and using the approximation technique of (9), the active damping filter is re-defined accordingly to be used in the root-locus calculation

$$F(s) = k_{ad}C_{cp} \frac{f_s(e^{s/f_s} - 1)}{e^{s/f_s}} \approx k_{ad}C_{cp} \frac{s}{1 + s/(2f_s)}. \quad (15)$$

As shown below, the active damping control action defined by (14)-(15) is able to shape the dynamics of the system (i.e., the placement of the dominant poles), despite its deviations from the ideal (anti-causal) filter and the effects of system delays [modeled by (9)-(11)].

#### IV. ROOT-LOCUS BASED TUNING DERIVED FROM THE IMPEDANCE/ADMITTANCE FORMULATION

Starting from the Impedance/Admittance Stability formulation, a systematic methodology to calculate the root locus and then tune the current controller is developed in this section.

By assuming that both  $Y_c(s)$  and  $Z_g(s)$  are open loop stable<sup>1</sup>, a modified sensitivity transfer function, which represents the dynamics of the closed loop system, is defined as

$$S_m(s) = \frac{1}{1 + Y_c(s)Z_g(s)}. \quad (16)$$

Then, the dominant poles of the closed-loop system are available from the  $S_m(s)$  root-locus.

In practice, since the LCL filter defines a poorly damped physical system, the dynamics are defined by an under-damped second order system. The dominant pair of poles is defined as  $p_{d\pm j}$ , with  $\text{Re}(p_{d\pm j})$  and  $\text{Im}(p_{d\pm j})$  being their real and imaginary parts. The dominant time constant is given by  $\tau_d = 1/\text{Re}(p_{d\pm j})$ . As shown below, in practice,  $\text{Im}(p_{d\pm j})$  is around  $\pm\omega_{res}$ , which provides physical meaning to the model: the roots associated to  $\omega_{res}$  oscillations limit the dynamics of the system. Furthermore, since the system is poorly damped, it is observed that  $|\text{Re}(p_{d\pm j})| < |\text{Im}(p_{d\pm j})|$ .

##### A. Control and Tuning Objectives

Besides a fast time response, reliability of the current controller when working in different grid conditions is a key objective, which is strongly related to the concepts of robustness and relative stability [31]–[33]. Robustness in terms of root-locus design can be formulated as follows: for a given nominal plant, the closed loop dominant poles should lie inside a predefined stability region [31]. For the wind turbine application, a maximum time constant  $\tau_{d,max}$  for the inner current controllers imposes the design objective: a constrained stability region is as depicted in Fig. 3. On the other hand, design for passivity methods also point to provide a robust solution in the presence of uncertainty in the grid. However, by definition, the region for stability implicitly considers the

<sup>1</sup>This condition is imposed to avoid unstable pole-zero cancellations [38].  $Z_c(s)$  is stable by definition.  $Y_c(s)$  stability can be checked in the design stage.

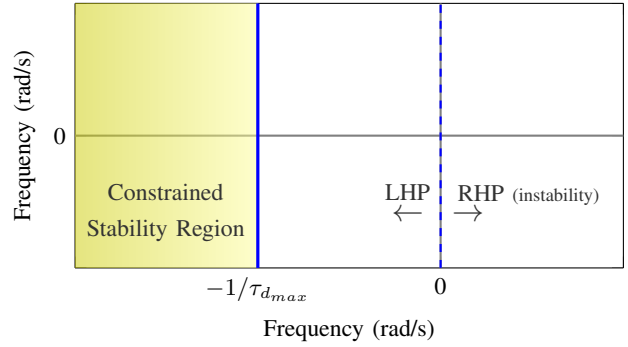


Fig. 3. Definition of a constrained stability region according to the wind turbine controller requirements.

whole left half plane (LHP), since absolute stability is the control objective (i.e., no poles in the RHP are allowed) [33]; hence, the region of stability imposed by the application (i.e., a minimum time response, as shown in Fig. 3) is more restrictive than the one imposed by design for passivity methods.

Therefore, the minimization of  $\tau_d$  for a given nominal grid  $Z_g(s)$ , is a design objective aligned with both time response and reliability of the grid-connected converter. By means of the root-loci information, the tuning objective is to find the collection of  $k_p$ ,  $k_i$  and  $k_{ad}$  parameters [in (5)] that fulfil the following criteria:

- 1) In order to minimize the current controller dominant time constant, given by  $\tau_d = 1/\text{Re}(p_{d\pm j})$ ,  $\text{Re}(p_{d\pm j})$  should lie in the LHP, as further as possible from the RHP.
- 2) The damping factor of the dominant poles, defined as

$$\xi_d = \frac{|\text{Re}(p_{d\pm j})|}{\sqrt{\text{Re}(p_{d\pm j})^2 + \text{Im}(p_{d\pm j})^2}} \quad (17)$$

should be maximized, which is achieved by increasing  $|\text{Re}(p_{d\pm j})|$ , with  $\text{Im}(p_{d\pm j}) \approx \pm\omega_{res}$  being a good approximation in practice. An insightful relation between phase margin (PM) and damping factor is given by  $PM \approx 100\xi_d$  [32]; i.e., the relative stability of the system is enhanced by increasing  $|\text{Re}(p_{d\pm j})|$ .

In sum, by maximizing  $|\text{Re}(p_{d\pm j})|$  both transient response and relative stability are enhanced.

#### V. CASE STUDY

The parameters of the lab-scale prototype used for experimental verification (next section) have been employed to develop the theoretical approaches in a case study. Table I shows the physical parameters employed for analysis and experimental verification, which aim to follow the design guidelines explained in section II-A. Since a key aspect of the analysis is to show how the active damping action changes the dynamics of the system, a relatively low resonance frequency is selected [16] (both in the analysis and in the experimental verification). It should be also noted that  $Z'_g(s)$  is neglected in the analysis, since  $|Z'_g(s)| \ll |L_{ts}s + R_{ts}|$  is an accurate assumption for low-power scale circuits (i.e., the leakage

TABLE I  
PHYSICAL SYSTEM PARAMETERS

Parameter	Value
Rated Power	$S = 2.2 \text{ kVA}$
Rated Voltage (Line to line RMS)	$V = 220 \text{ V}$
Sampling (and PWM switching) frequency	$f_s = 10 \text{ kHz} (\omega_s = 2\pi f_s)$
Converter inductance	$L_{cs} = 8.6 \text{ mH} (0.123 \text{ p.u.})$
Converter equivalent resistance	$R_{cs} = 0.27 \Omega (0.012 \text{ p.u.})$
Capacitor	$C_{cp} = 4.5 \text{ uF} (0.039 \text{ p.u.})$
Capacitor ESR	$R_{cp} = 1 \text{ m}\Omega (< 0.001 \text{ p.u.})$
Grid Side Inductance	$L_{gs} = 4.7 \text{ mH} (\text{trafo leakage}) + 1.8 \text{ mH} = 6.8 \text{ mH} (0.097 \text{ p.u.})$
Grid Side Resistor	$R_{gs} = 0.22 \Omega (0.010 \text{ p.u.})$
LCL resonance frequency	$\omega_{res} = 7743 \text{ rad/s} (f_{res} = 1.233 \text{ kHz})$
Latency (1 sample in dSpace DS1006)	$t_L = 1/f_s = 100 \mu\text{s}$
PWM/ZOH delay	$t_{pwm} = 0.5/f_s = 50 \mu\text{s}$

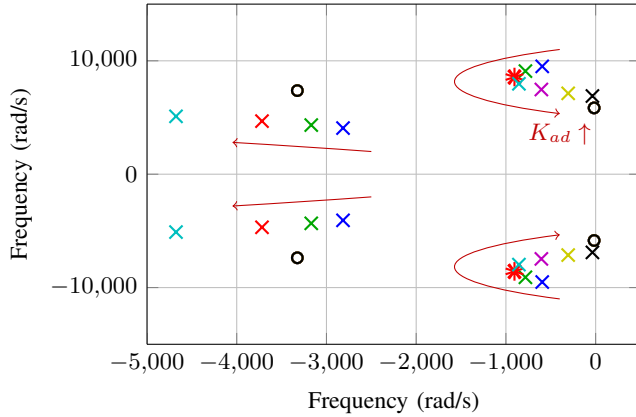


Fig. 4. “Moderate  $\alpha_c$ ” tuning: root-locus by a  $k_{ad}$  sweep with  $\alpha_c = 0.05\omega_s$ .

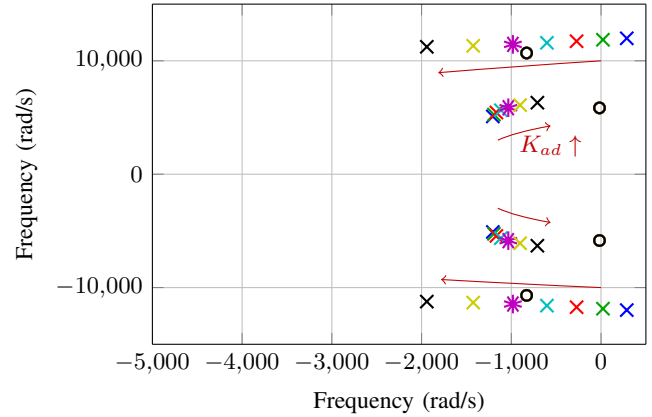


Fig. 5. “High  $\alpha_c$ ” tuning: root-locus by a  $k_{ad}$  sweep with  $\alpha_c = 0.1\omega_s$ .

inductor of a low power transformer is much higher than other impedances in the path of the stiff grid).

Different methodologies to get the tunings that accomplish the application objectives have been performed as explained below.

#### A. Tuning by Inspection

A criterion to start the tuning is first to consider that the dominant roots mainly depend on the proportional constant  $k_p$  [9], [10], [28]. The proportional constant is re-written as

$$k_p = (L_{cs} + L_{ts})\alpha_c \quad (18)$$

with  $\alpha_c$  being the theoretical closed loop bandwidth [16], [20], [28]. The main reason to use this expression is to give physical insight to the  $k_p$  parameter [11], [28]. By means of a  $\alpha_c$  ( $k_p$ ) sweep (with  $k_i = k_{ad} = 0$ ), it has been found that the real part of the dominant poles is maximized at  $\alpha_c = 0.05\omega_s$ . This gain can be considered a moderate one when compared to the maximum value defined by the one-to-tenth-rule, i.e.,  $0.1\omega_s$  [45]. Therefore, this tuning is named “moderate  $\alpha_c$ ”.

Subsequently, the gain of  $k_i$  is introduced: a relatively low  $k_i$  does not give a significant change in the root locus; i.e.,

- the new roots result in pole-zero cancellations around  $j\omega_1$  (resonant gains) so the system order is kept.

- The effect  $k_i$  on the main roots is relatively small; i.e., as expected  $k_p$  weights much more in the dominant poles placement.

It should be mentioned that, this reasoning applies in all the tunings;  $k_i = 5000$  has been employed in all the root-loci (and in the experiments).

Subsequently, a  $k_{ad}$  sweep, which shown in Fig. 4, seeks to identify the most convenient gain that maximizes the real magnitude of the dominant poles. The dominant poles that give the most convenient tuning (according to the proposed control objectives) are highlighted in red in Fig. 4; the parameters are  $\alpha_c = 0.05\omega_s$ ,  $k_i = 5000$  and  $k_{ad} = 10$ . The dominant poles obtained with the “moderate  $\alpha_c$ ” tuning are  $p_{d\pm j} = -905 \pm 8570 \text{ rad/s}$ .

Another criterion to start the tuning is by considering that the active damping is more effective changing the position of the dominant poles when the main controller has a high theoretical bandwidth [16]. This suggests that another tuning strategy starting from  $\alpha_c = 0.1\omega_s$  (one-to-tenth rule [45]). Fig. 5 shows the root-locus based on a  $k_{ad}$  for  $\alpha_c = 0.1\omega_s$ . This tuning is named “high  $\alpha_c$ ”. It can be noticed that the system is unstable if active damping is not activated ( $k_{ad} = 0$ ). With  $k_{ad} = 20$  there is two sets of pair of poles with  $\text{Re}(p_{d\pm j}) \approx -1000 \text{ rad/s}$  (i.e., a fourth order dominant response); in Fig. 5, these roots are highlighted in purple.

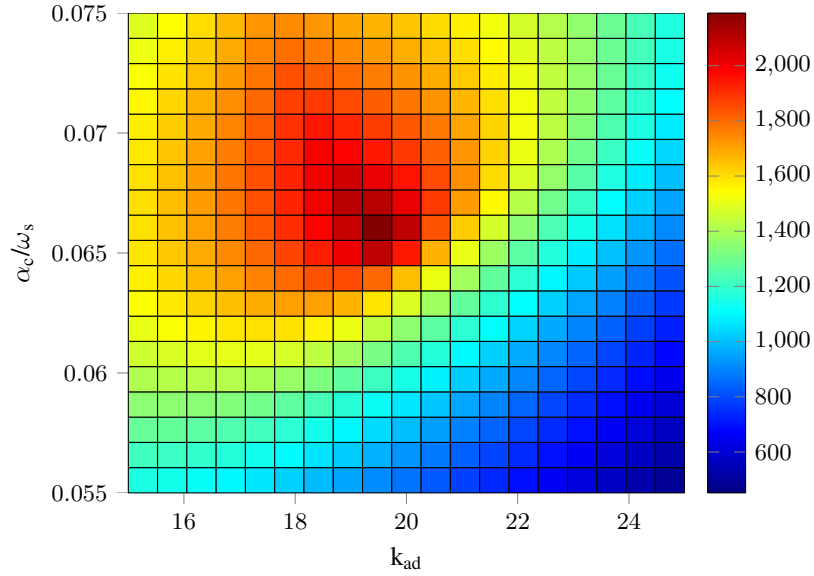


Fig. 6. Surface plot showing the results of the direct search in the  $\alpha_c - k_{ad}$  axes. The gradient colors represent  $|\text{Re}(p_{d_{\pm j}})|$ . The optimal solution (i.e., “optimal” tuning) is identified at  $(\alpha_c = 0.066\omega_s, k_{ad} = 19.5)$ .

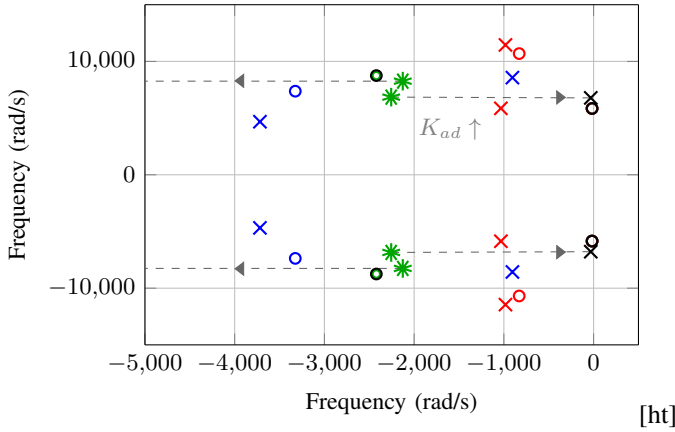


Fig. 7. Root-loci of the analyzed tunings: (blue) “moderate  $\alpha_c$ ”; (red) “high  $\alpha_c$ ”; (green) “optimum”; (black) “high  $k_{ad}$ ”. The dashed arrow represents the trajectories of the poles from the “optimal” tuning to “high  $k_{ad}$ ” one as  $k_{ad}$  increases.

### B. “Optimal” Tuning

From the previous sections it can be seen that, overall, a moderate  $\alpha_c$  is convenient to initially move the dominant poles to the left, but the tuning of  $k_{ad}$  is more effective for higher  $\alpha_c$  values. Therefore, it is expected that there is an optimum set of  $(\alpha_c, k_{ad})$  values that places the dominant poles the furthest away from the RHP. This problem can be solved by finding the minimum of  $\text{Re}(p_{d_{\pm j}})$  [i.e., the maximum of  $|\text{Re}(p_{d_{\pm j}})|$  for stable solutions] in the  $(\alpha_c, k_{ad})$  plane, which has been obtained by a direct search method [46]: Fig. 6 depicts  $|\text{Re}(p_{d_{\pm j}})|$  for a bounded set of  $(\alpha_c, k_{ad})$  that assures stability. The optimal solution is obtained with  $\alpha_c = 0.066\omega_s$  and  $k_{ad} = 19.5$ , where  $|\text{Re}(p_{d_{\pm j}})| \approx 2150$  rad/s.

Fig. 7 shows the different root-loci, including the “optimal” tuning (highlighted in green), which gives two set of dominant pair of poles with  $|\text{Re}(p_{d_{\pm j}})| \approx 2150$  rad/s. A solution with

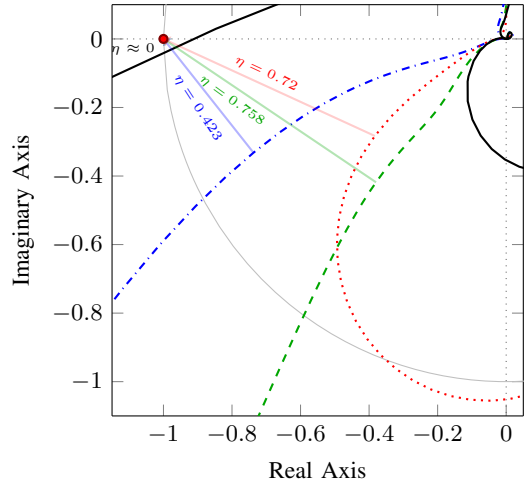


Fig. 8. Nyquist trajectories corresponding to Fig. 7: (dashed-dotted blue) “moderate  $\alpha_c$ ”; (dotted red) “high  $\alpha_c$ ”; (dashed green) “optimum”; (solid black) “high  $k_{ad}$ ”.

$\alpha_c = 0.066\omega_s$  but high  $k_{ad}$  is also represented in order to show how a high  $k_{ad}$  drives the system to near to the RHP (instability). The latest tuning is named “high  $k_{ad}$ ”.

Fig. 7 also represents the zeros of  $S_m(s)$ , including the ones relatively close to the dominant poles. As shown in the experimental section, these zeros have influence on the dynamics as they mitigate the amplitude associated to the dominant responses in the command step response.

### C. Correspondence with Nyquist Diagrams

Fig. 8 represents the Nyquist trajectories corresponding to the root-loci of Fig. 7. Overall, it can be appreciated that the “moderate  $\alpha_c$ ”, “high  $\alpha_c$ ” and “optimum” tunings provide low sensitivity peaks, defined by  $1/\eta$  for each trajectory [6], [38], [47]. Low sensitivity peak means good relative stability; on

TABLE II  
 $|Y_c(j\omega)|$  AT THE LOW FREQUENCY REGION (GRID VOLTAGE HARMONICS REJECTION)

Tuning	$Y_c(j\omega = 0)$ [dB]	$Y_c(j\omega = 0)$ [ $\Omega^{-1}$ ]	$1/k_p$ [ $\Omega^{-1}$ ]
“Moderate $\alpha_c$ ”	-33.57	0.0210	0.0213 ( $k_p = 47$ )
“High $\alpha_c$ ”	-39.86	0.0102	0.0102 ( $k_p = 98$ )
“Optimum”	-36.46	0.0150	0.0152 ( $k_p = 66$ )

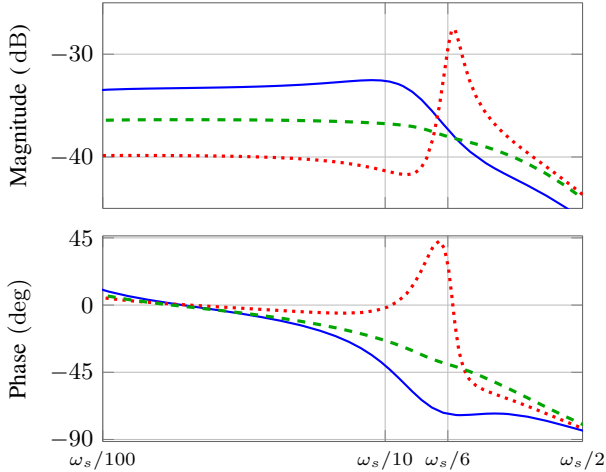


Fig. 9. Frequency Response of  $Y_c(j\omega)$  for different tunings: (solid blue) “moderate  $\alpha_c$ ”; (dotted red) “high  $\alpha_c$ ”; (dashed green) “optimum”.

the contrary, the “high  $k_{ad}$ ” gives a high sensitivity peak; i.e., low conditional stability [6], [38], [47]. However, it can be appreciated the calculation of  $p_{d\pm j}$  (including potential pole-zero cancelations) is not so straightforward by inspection of the Nyquist trajectories [6].

#### D. $Y_c(j\omega)$ Shape and Disturbance Rejection

From the definition in (4),  $Y_c(j\omega)$  represents the converter current due to the presence of grid voltage harmonics. For perfect reference tracking and disturbance rejection,  $Y_c(j\omega) = 0$  should be the design objective [28]. In practice, this objective is fulfilled at some specific frequencies (e.g., low order odd harmonics) by means of resonant filters [9], [10], [28]. However, resonant filters are very selective, so at the rest of frequencies inside the controller bandwidth (i.e.,  $\omega < \omega_s/10$ ),  $Y_c(j\omega)$  mainly depends on the proportional gain  $k_p$ . More specifically, from (5), it is straightforward to derive  $|Y_c(j\omega)| \approx 1/k_p$  for the low frequency range, where  $L_{cs}\omega \ll k_p$  and  $k_{ad}C_{cp}\omega \ll 1$  are accurate assumptions. Fig. 9 shows the frequency response of  $Y_c(j\omega)$  for the key tunings analyzed in this section. It can be appreciated how the low frequency approximation to predict the disturbance rejection effectiveness is accomplished. As expected, the higher gain tuning provides a higher disturbance rejection, as also summarized in Table II.

At a higher frequency range, stability properties can be also estimated from the  $Y_c(j\omega)$  frequency response [27]. In this case, due to the active damping action, absolute stability is expected for all the systems, since none of them presents  $-90$ deg phase crosses in the vicinity of  $\omega_s/6$ , a critical

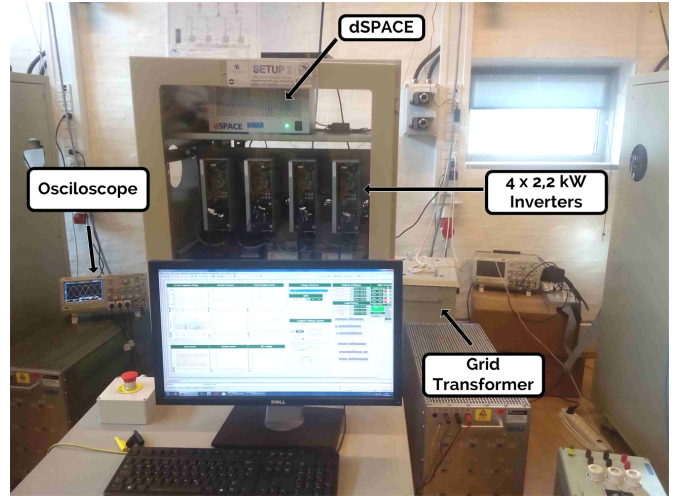


Fig. 10. Lab set-up photography.

frequency as identified in [19], [20]. However, it may be also noticed that the “high  $\alpha_c$ ” provides a magnitude peak around  $\omega_s/6$ , which, in principle, would compromise the stability (i.e., a magnitude increment of the Nyquist trajectory) [27]. These observations explain how an increment on  $k_p$  artificially excites the system resonance, and then the active damping can re-stabilizes it [16].

## VI. EXPERIMENTAL RESULTS

The experimental verification has been carried out in the test-bed shown in Fig. 10. The objective of the experimental verification is to show that the “optimal” tuning derived from the theoretical analysis, provides a damped and fast dynamic response, while limiting the harmonic amplification of the LCL filter around  $\omega_{res}$ . According to the theoretical analysis, and given the parameters of the test-bed, the optimal tuning is obtained for  $\alpha_c = 0.066\omega_s$  and  $k_{ad} = 19.5$ . Subsequently, as the lab-scale is by nature a highly damped system [16], [48], control gains can be used to artificially undamp it [16]. From the theoretical analysis, it can be appreciated that  $k_{ad}$  has a greater impact on the system stability: an increment of  $k_{ad}$  moves the dominant poles near the instability region (cf., “high  $k_{ad}$ ” tuning in Fig. 7). In order to test the accuracy of the theoretical analysis, experimental results with a “high  $k_{ad}$ ” tuning are shown. It is proved how the proposed method is able to accurately calculate the control gains that lead the system near the instability region.

Fig. 11 shows the grid current  $i_g(t)$  during steps of amplitude  $5A$  in the converter active current command (some reactive current flows the LCL capacitor when the converter current is zero). Fig. 11(a) shows the response for optimal

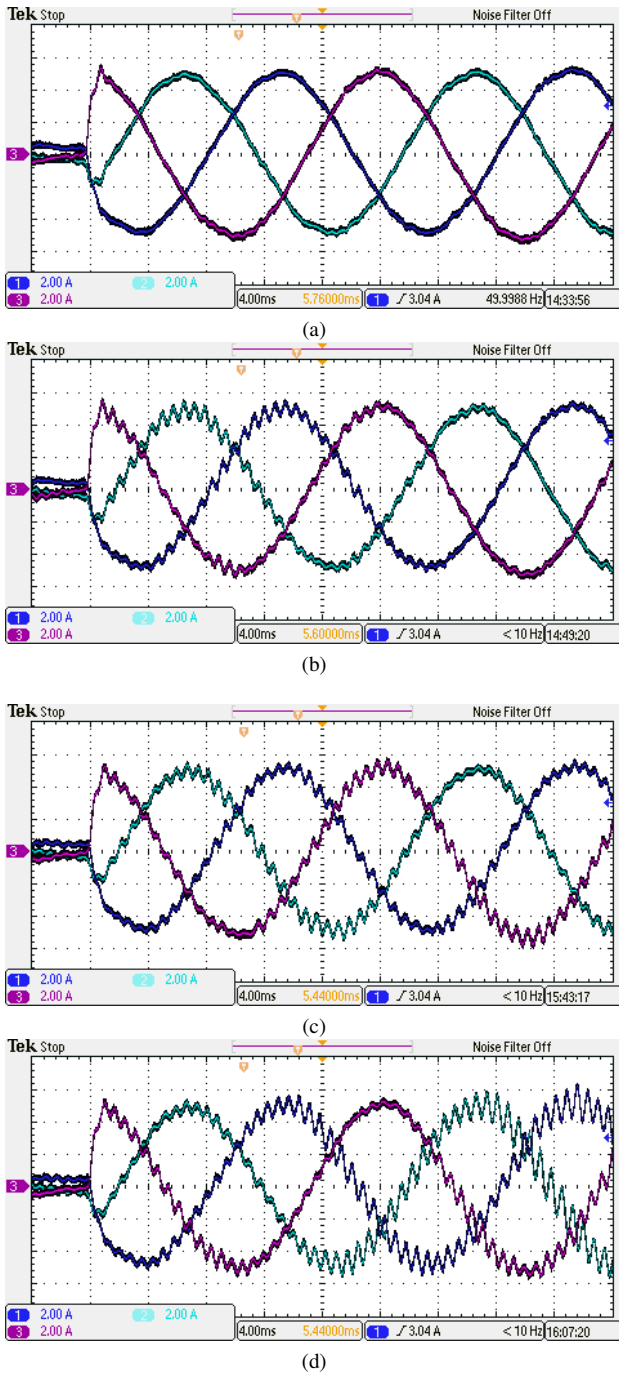


Fig. 11. Active current step test. (a)  $k_{ad} = 19.5$  and  $\alpha_c = 0.066\omega_s$  (optimal tuning). (b)  $k_{ad} = 34$  and  $\alpha_c = 0.066\omega_s$  (“high  $k_{ad}$ ” tuning 1). (c)  $k_{ad} = 35$  and  $\alpha_c = 0.066\omega_s$  (“high  $k_{ad}$ ” tuning 2). (d)  $k_{ad} = 36$  and  $\alpha_c = 0.066\omega_s$  (“high  $k_{ad}$ ” tuning 3).

tuning (the dominant poles are represented in green in Fig. 7): as expected, the system response shows a fast step response with little steady-state distortion. Figs. 11(b)-11(d) show the response when the active damping constant is increased so the dominant poles are near the RHP (the dominant poles are represented in black in Fig. 7, which corresponds to the named “high  $k_{ad}$ ” tuning). Three different scenarios are considered to highlight the high influence of  $k_{ad}$  in the current control dynamics. In all these cases, an oscillation of a frequency

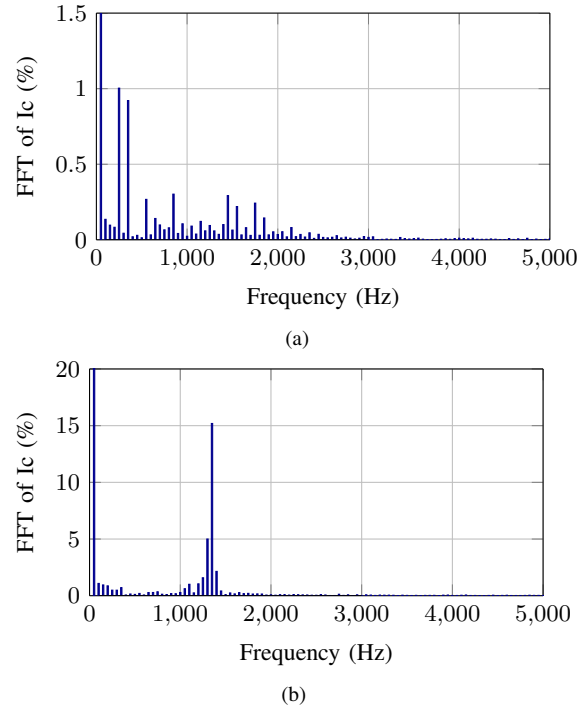


Fig. 12. Harmonic spectrum with (a)  $k_{ad} = 19.5$  and  $\alpha_c = 0.066\omega_s$  (optimal tuning); the THD is 1.6%. (b)  $k_{ad} = 35$  and  $\alpha_c = 0.066\omega_s$  (“high  $k_{ad}$ ” tuning 2); the THD is 16.3%.

around  $\omega_{res}$  (defined by the LCL filter parameters) is observed, which is also predicted in Fig. 7 (i.e., the imaginary part of the dominant poles in Fig. 7 is around 6500 rad/s, a value similar but slightly smaller than  $\omega_{res}$ ). Fig. 11(b) shows that the oscillation decays with a slow time constant in comparison to the initial response. Fig. 11(c) shows that the oscillation is self-sustained as  $k_{ad} = 35$ , which means that the system behaves as marginally stable. Fig. 11(d) shows that the system becomes unstable at  $k_{ad} = 36$ , as the amplitude of the oscillation increases with time<sup>2</sup>. It can be appreciated that the experimental verification is in a good agreement with the theoretical analysis, and the different tests well match the predictions obtained by the  $S_m(s)$  root-loci of Fig. 7, which proves the main theoretical hypothesis.

Fig. 12 shows the  $i_g(t)$  harmonic spectrum for  $k_{ad} = 19.5$  and  $k_{ad} = 35$  that corresponds to Fig. 11(a) and Fig. 11(c) steady-state waveforms. As expected from the “optimal” tuning, the dominant poles have maximized its damping factor [see also (17)], so the harmonic components around  $f_{res}$  are small. The most relevant harmonics are the 5<sup>th</sup> and 7<sup>th</sup> of about a 1% and the total harmonic distortion (THD) is 1.6%. For Fig. 11(c), there is a 15% component associated to the LCL resonance (see  $f_{res}$  region): the THD increases up to 16.3% because of these harmonics.

<sup>2</sup>It can be noticed that the system passive damping also changes when the step is activated: the converter has more efficiency when the active current reference is close to its nominal conditions and hence, passive damping is reduced [48].

## VII. CONCLUSIONS

This paper contributes an original methodology for systematic analysis and design of current controllers for LCL grid-connected VSCs, with special emphasis on wind turbine applications. The proposed approach is derived from the impedance/admittance stability criterion, which eases the design of controllers with active damping and, on the other hand, is suitable for modeling the wind turbine in system level studies. The main control objective is formulated as a minimization of the current control dominant time constant, in accordance with standard procedures for wind turbine controller design and also enhancing the relative stability to deal with potential uncertainties in the grid model. A modified sensitivity transfer function, expressed in form of  $Y_c(s)$  and  $Z_g(s)$ , is provided in order to calculate the system root loci. From the theoretical case study, it is shown how both  $\alpha_{cc} (k_p)$  and  $k_{ad}$  influence the dynamics, and how an optimal solution to the control problem can be obtained by direct search. The experimental results validate the proposed methodology by means of time and frequency domain key figures. The analysis and verification are mainly provided for a given nominal design of LCL grid-connected VSC. Future works would further explore the robustness of the technique in more realistic scenarios (e.g., using data from a wind power plant).

## REFERENCES

- [1] S. S. Sheng, "Report on wind turbine subsystem reliability – a survey of various databases," NREL, Tech. Rep., 2013.
- [2] T. Neumann, T. Wijnhoven, G. Deconinck, and I. Erlich, "Enhanced dynamic voltage control of type 4 Wind turbines during unbalanced grid faults," *IEEE Trans. Energy Convers.*, vol. 30, no. 4, pp. 1650–1659, Dec. 2015.
- [3] F. D. Bianchi, H. De Battista, and R. J. Mantz, *Wind turbine control systems: principles, modelling and gain scheduling design*. Springer Science & Business Media, 2006.
- [4] E. Van der Hoof, P. Schaak, and T. Van Engelen, "Wind turbine control algorithms (DOWEC-F1W1-EH-03-094/0)," T. U. Delft., Tech. Rep., 2003.
- [5] M. H. Hansen, A. Hansen, T. J. Larsen, S. Oye, P. Sorensen, and P. Fuglsang, "Control design for a pitch-regulated, variable speed wind turbine. Riso-R-1500(EN)," Riso National Laboratory, Tech. Rep., 2005.
- [6] K. Astrom and T. Hagglund, *PID Controllers: Theory, Design and Tuning, Second Edition*. Instrument Society of America, 1995, pp. 274–279.
- [7] F. Shinsky, B. Liptak, R. Bars, and J. Hetthessy, "2.6 Control Systems–Cascade Loops," in *Process Control and Optimization, Volume II*. ISA, Taylor Francis, 2006, pp. 148–156.
- [8] R. Teodorescu, M. Liserre, and P. R. Rodriguez, *Grid converters for photovoltaic and wind power systems*. John Wiley & Sons, 2011, vol. 29.
- [9] A. Vidal, F. D. Freijedo, A. G. Yepes, P. Fernandez-Comesana, J. Malvar, O. Lopez, and J. Doval-Gandoy, "Assessment and optimization of the transient response of proportional-resonant current controllers for distributed power generation systems," *IEEE Trans. Ind. Electron.*, vol. 60, no. 4, pp. 1367–1383, Apr. 2013.
- [10] A. Vidal, F. D. Freijedo, A. G. Yepes, J. Malvar, O. Lopez, and J. Doval-Gandoy, "Transient response evaluation of stationary-frame resonant current controllers for grid-connected applications," *IET Power Electronics*, vol. 7, no. 7, pp. 1714–1724, 2014.
- [11] F. D. Freijedo, A. Vidal, A. G. Yepes, J. M. Guerrero, O. Lopez, J. Malvar, and J. Doval-Gandoy, "Tuning of synchronous-frame PI current controllers in grid-connected converters operating at a low sampling rate by MIMO root locus," *IEEE Trans. Ind. Electron.*, vol. 62, no. 8, pp. 5006–5017, 2015.
- [12] A. Timbus, M. Liserre, R. Teodorescu, P. Rodriguez, and F. Blaabjerg, "Evaluation of Current Controllers for Distributed Power Generation Systems," *IEEE Trans. Power Electron.*, vol. 24, no. 3, pp. 654–664, Mar. 2009.
- [13] J. C. Ausin, D. N. Gevers, and B. Andresen, "Fault ride-through capability test unit for wind turbines," *Wind Energy*, vol. 11, no. 1, pp. 3–12, 2008.
- [14] G. Gohil, L. Bede, R. Teodorescu, T. Kerekes, and F. Blaabjerg, "Line filter design of parallel interleaved vscs for high-power wind energy conversion systems," *IEEE Trans. Power Electron.*, vol. 30, no. 12, pp. 6775–6790, 2015.
- [15] R. Pena-Alzola, M. Liserre, F. Blaabjerg, R. Sebastian, J. Dannehl, and F. Fuchs, "Analysis of the passive damping losses in LCL-filter-based grid converters," *IEEE Trans. Power Electron.*, vol. 28, no. 6, pp. 2642–2646, 2013.
- [16] J. Dannehl, F. Fuchs, S. Hansen, and P. Thogersen, "Investigation of active damping approaches for pi-based current control of grid-connected pulse width modulation converters with LCL filters," *IEEE Trans. Ind. Appl.*, vol. 46, no. 4, pp. 1509–1517, 2010.
- [17] L. Harnefors, A. G. Yepes, A. Vidal, and J. Doval-Gandoy, "Passivity-based stabilization of resonant current controllers with consideration of time delay," *IEEE Trans. Power Electron.*, vol. 29, no. 12, pp. 6260–6263, 2014.
- [18] R. Pena-Alzola, M. Liserre, F. Blaabjerg, M. Ordonez, and Y. Yang, "LCL-filter design for robust active damping in grid-connected converters," *IEEE Trans. Ind. Informat.*, vol. 10, no. 4, pp. 2192–2203, 2014.
- [19] S. Parker, B. McGrath, and D. Holmes, "Regions of active damping control for LCL filters," *IEEE Trans. Ind. Appl.*, vol. 50, no. 1, pp. 424–432, 2014.
- [20] L. Harnefors, A. G. Yepes, A. Vidal, and J. Doval-Gandoy, "Passivity-based controller design of grid-connected vscs for prevention of electrical resonance instability," *IEEE Trans. Ind. Electron.*, vol. 62, no. 2, pp. 702–710, 2015.
- [21] D. Yang, X. Ruan, and H. Wu, "Impedance shaping of the grid-connected inverter with LCL filter to improve its adaptability to the weak grid condition," *IEEE Trans. Power Electron.*, vol. 29, no. 11, pp. 5795–5805, 2014.
- [22] J. Wang, J. Yan, and L. Jiang, "Pseudo-derivative-feedback current control for three-phase grid-connected inverters with LCL filters," *IEEE Trans. Power Electron.*, vol. 31, no. 5, pp. 3898–3912, 2016.
- [23] J. Wang, J. D. Yan, L. Jiang, and J. Zou, "Delay-dependent stability of single-loop controlled grid-connected inverters with LCL filters," *IEEE Trans. Power Electron.*, vol. 31, no. 1, pp. 743–757, 2016.
- [24] Z. Xin, P. Loh, X. Wang, F. Blaabjerg, and Y. Tang, "Highly accurate derivatives for LCL-filtered grid converter with capacitor voltage active damping," *IEEE Trans. Power Electron.*, vol. 31, no. 5, pp. 3612–3625, 2016.
- [25] *IEC 61400-21 Ed.2, Wind turbines – Part 21: Measurement and assessment of power quality characteristics of grid connected wind turbines*, IEC Std., Feb. 2007.
- [26] L. Harnefors, M. Bongiorno, and S. Lundberg, "Input-admittance calculation and shaping for controlled voltage-source converters," *IEEE Trans. Ind. Electron.*, vol. 54, no. 6, pp. 3323–3334, 2007.
- [27] J. Sun, "Impedance-based stability criterion for grid-connected inverters," *IEEE Trans. Power Electron.*, vol. 26, no. 11, pp. 3075–3078, 2011.
- [28] L. Harnefors, L. Zhang, and M. Bongiorno, "Frequency-domain passivity-based current controller design," *IET Power Electron.*, vol. 1, no. 4, pp. 455–465, Dec. 2008.
- [29] F. Wang, J. L. Duarte, M. A. M. Hendrix, and P. F. Ribeiro, "Modeling and analysis of grid harmonic distortion impact of aggregated dg inverters," *IEEE Transactions on Power Electronics*, vol. 26, no. 3, pp. 786–797, Mar. 2011.
- [30] H. Kocewiak, J. Hjerrild, and C. Bak, "Wind turbine converter control interaction with complex wind farm systems," *IET Renewable Power Generation*, vol. 7, no. 4, pp. 380–389, 2013.
- [31] S. Bhattacharyya, H. Chapellat, and L. Keel, *Robust control: the parametric approach*. Prentice-Hall, 1995.
- [32] R. C. Dorf and R. H. Bishop, *Modern Control Systems*, ., Ed. Prentice Hall, 2007.
- [33] E. Mollerstedt and B. Bernhardsson, "Out of control because of harmonics-an analysis of the harmonic response of an inverter locomotive," *IEEE Control Syst. Mag.*, vol. 20, no. 4, pp. 70–81, 2000.
- [34] N. Strachan and D. Jovicic, "Stability of a variable-speed permanent magnet wind generator with weak AC grids," *IEEE Trans. Power Del.*, vol. 25, no. 4, pp. 2779–2788, 2010.
- [35] A. Golieva, "Low short-circuit ratio connection of wind power plants," Master's thesis, Norwegian University of Science and Technology, 2015.

- [36] J. Dannehl, M. Liserre, and F. Fuchs, "Filter-based active damping of voltage source converters with filter," *IEEE Trans. Ind. Electron.*, vol. 58, no. 8, pp. 3623–3633, 2011.
- [37] S. Skogestad and I. Postlethwaite, *Multivariable Feedback Control*. Wiley, 2005, pp. 27, 67–71, 119–154.
- [38] G. C. Goodwin, S. F. Graebe, and M. E. Salgado, *Control System Design*. Prentice Hall, 2000.
- [39] M. Cespedes and J. Sun, "Impedance modeling and analysis of grid-connected voltage-source converters," *IEEE Trans. Power Electron.*, vol. 29, no. 3, pp. 1254–1261, 2014.
- [40] B. Wen, D. Dong, D. Boroyevich, R. Burgos, P. Mattavelli, and Z. Shen, "Impedance-based analysis of grid-synchronization stability for three-phase paralleled converters," *IEEE Trans. Power Electron.*, vol. 31, no. 1, pp. 26–38, 2016.
- [41] L. Harnefors, "Modeling of three-phase dynamic systems using complex transfer functions and transfer matrices," *IEEE Trans. Ind. Electron.*, vol. 54, no. 4, pp. 2239–2248, Aug. 2007.
- [42] B. Wen, D. Boroyevich, R. Burgos, P. Mattavelli, and Z. Shen, "Analysis of d-q small-signal impedance of grid-tied inverters," *IEEE Trans. Power Electron.*, vol. 31, no. 1, pp. 675–687, 2016.
- [43] A. Yepes, F. Freijedo, J. Doval-Gandoy, O. Lopez, J. Malvar, and P. Fernandez-Comesana, "Effects of discretization methods on the performance of resonant controllers," *IEEE Trans. Power Electron.*, vol. 25, no. 7, pp. 1692–1712, 2010.
- [44] K. Sozanski, *Digital Signal Processing in Power Electronics Control Circuits*. Springer Verlag, 2013.
- [45] S. Buso and P. Mattavelli, *Digital Control in Power Electronics*. Morgan and Claypool, 2006.
- [46] R. M. Lewis, V. Torczon, and M. W. Trosset, "Direct search methods: then and now," *Journal of computational and Applied Mathematics*, vol. 124, no. 1, pp. 191–207, 2000.
- [47] A. Yepes, F. Freijedo, O. Lopez, and J. Doval-Gandoy, "Analysis and design of resonant current controllers for voltage source converters by means of nyquist diagrams and sensitivity function," *IEEE Trans. Ind. Electron.*, vol. 58, no. 11, pp. 5231 – 5250, 2011.
- [48] A. Vidal, A. Yepes, F. Freijedo, O. Lopez, J. Malvar, F. Baneira, and J. Doval-Gandoy, "A method for identification of the equivalent inductance and resistance in the plant model of current-controlled grid-tied converters," *IEEE Trans. Power Electron.*, vol. 30, no. 12, pp. 7245–7261, 2015.



**Francisco D. Freijedo (M'07-SM'16)** received the M.Sc. degree in physics from the University of Santiago de Compostela, Santiago de Compostela, Spain, in 2002 and the Ph.D. degree in electrical engineering from the University of Vigo, Vigo, Spain, in 2009. From 2005 to 2011, he was a Lecturer in the Department of Electronics Technology, University of Vigo. From 2011 to 2014, he worked with Gamesa Innovation and Technology as a Power Electronics Control Engineer for renewable energy applications. From 2014 to 2016, he was a

Postdoctoral Researcher in the Department of Energy Technology, Aalborg University. Since 2016, he is a Scientific Collaborator of the Power Electronics Laboratory, Ecole Polytechnique Federale de Lausanne. His main research interests include power conversion technologies.



**Enrique Rodriguez (S'15)** earned his B.S. degree in electronics engineering and his M.S. degree in sustainable transportation and electrical power systems from the University of Oviedo, Spain, in 2012 and 2014, respectively. He is currently working toward his Ph.D. degree in energy technology at Aalborg University, Denmark. He is a member of the International Electrotechnical Commission System Evaluation Group SEG4 on Low-Voltage dc Applications, Distribution, and Safety for use in Developed and Developing Economies. His research interests are

low-voltage distribution systems, control of power converter units, energy-management systems, and microgrids.



**Mohammad S. Golsorkhi (S'13)** received the B.Sc. (Hons.) degree from Isfahan University of Technology, Isfahan, Iran, in 2009, the M.Sc. (Hons.) degree from Tehran Poly-technique, Tehran, Iran, in 2012 and the PhD degree from the University of Sydney, Sydney, Australia in 2016, all in electrical engineering. During 2011–2012, he worked for Behrad consulting engineers as a R&D engineer. In 2015, he was a visiting PhD student with the Department of Energy Technology, Aalborg University, Denmark. He is currently a post-doctoral fellow in the Department of Electrical and Electronic Engineering, the University of Hong Kong, Hong Kong. His main research interests include control of microgrids, renewable energy resources, and power electronics.



**Juan C. Vasquez (M'12-SM'14)** received the B.S. degree in electronics engineering from the Autonomous University of Manizales, Manizales, Colombia, and the Ph.D. degree in automatic control, robotics, and computer vision from the Technical University of Catalonia, Barcelona, Spain, in 2004 and 2009, respectively. He was with the Autonomous University of Manizales working as a teaching assistant and the Technical University of Catalonia as a Post-Doctoral Assistant in 2005 and 2008 respectively. In 2011, he was Assistant

Professor and from 2014 he is working as an Associate Professor at the Department of Energy Technology, Aalborg University, Denmark where he is the Vice Programme Leader of the Microgrids Research Program. From Feb. 2015 to April. 2015 he was a Visiting Scholar at the Center of Power Electronics Systems (CPES) at Virginia Tech. His current research interests include operation, advanced hierarchical and cooperative control, optimization and energy management applied to distributed generation in AC and DC microgrids. He has authored and co-authored more than 100 technical papers only in Microgrids where 60 of them are published in international IEEE journals. Dr. Vasquez is currently a member of the IEC System Evaluation Group SEG4 on LVDC Distribution and Safety for use in Developed and Developing Economies, the Renewable Energy Systems Technical Committee TC-RES in IEEE Industrial Electronics, PELS, IAS, and PES Societies.



**Josep M. Guerrero (S'01-M'04-SM'08-FM'15)** received the B.S. degree in telecommunications engineering, the M.S. degree in electronics engineering, and the Ph.D. degree in power electronics from the Technical University of Catalonia, Barcelona, in 1997, 2000 and 2003, respectively. Since 2011, he has been a Full Professor with the Department of Energy Technology, Aalborg University, Denmark, where he is responsible for the Microgrid Research Program. From 2012 he is a guest Professor at the Chinese Academy of Science and the Nanjing

University of Aeronautics and Astronautics; and from 2014 he is chair Professor in Shandong University. His research interests is oriented to different microgrid aspects, including power electronics, distributed energy-storage systems, hierarchical and cooperative control, energy management systems, and optimization of microgrids and islanded minigrids. In 2014 he was awarded by Thomson Reuters as ISI Highly Cited Researcher, and in 2015 same year he was elevated as IEEE Fellow for contributions to distributed power systems and microgrids.